Article

Bifunctional SERS Paper Chips Based on Three-Layered Plasmonic Metal-Coated ZnO Nanoflowers for Fast Enrichment and Ultrasensitive Detection of Multiple Antibiotics

Juanjuan Yan,[#] Morui Wang,[#] Huaiqin Yin,[#] Mengmeng Ma, Yuee Li,* Haiyuan Hu, Weichun Ye,* Yumin Li,* and Hua Zhang*

ACCESS | Metrics & More | Article Recommendations | Supporting Information

ABSTRACT: In this study, cellulose filter paper (CFP) was used to create three-dimensional ZnO nanoflowers coated with three-layered plasmonic metals (Ag@Au@Ag) by using an in situ generated method. The substrate was created as a surface-enhanced Raman scattering (SERS) paper chip with dual functions for quick enrichment and ultrasensitive antibiotic detection. It was possible to detect amoxicillin, ciprofloxacin, and tetracycline quantitatively with good linear responses at low detection limits of 1, 10, and 10 nM, respectively, thanks to the characteristics of three-dimensional nanostructures, the charge transfer effect of ZnO−plasmonic metal, and electromagnetic coupling of Ag@Au@Ag. Even with a paper chip and a mobile phone−Raman spectrometer integrated system,

it was possible to identify human urine antibiotics at ppb levels with high accuracy. Meanwhile, 10 min detection of the antibiotics was accomplished by merely soaking them in their analyte solutions due to CFP wicking. With the help of PCA-LDA analysis, the multiplexed SERS spectral data of the three antibiotics could be successfully separated. Additionally, the paper chip's exceptional mechanical endurance even against 30-fold and strong ultrasonication was made possible by the in situ growing method. The bifunctional, affordable, and long-lasting SERS paper chip has a lot of potential for on-site and point-of-care drug detection.

KEYWORDS: surface-enhanced Raman scattering, flexible paper chip, three-layered plasmonic nanostructures, multiple detection, antibiotics
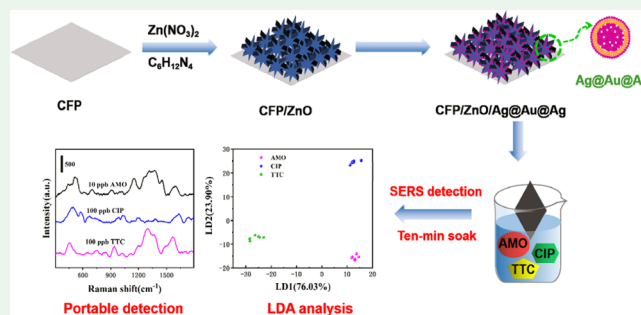
INTRODUCTION

Antibiotics hold a broad spectrum of activities against several Gram-negative and -positive bacteria.[1] They are extensively prescribed to treat bacterial infections and are available for oral administration.[2] However, antibiotics after metabolism in body tissues are excreted mostly as the parent compound in urine. Their overuse and abuse may link to multiple health hazards to humans, such as bone marrow suppression, hepatotoxicity, carcinogenic, and genotoxic.[3,4] Generally, several antibiotics are simultaneously taken for strong treatment activity, such as amoxicillin (AMO), ciprofloxacin (CIP), and tetracycline (TTC). Therefore, monitoring multiple antibiotics in urine rapidly, efficiently, and simultaneously is critical for the appropriate guidance to antibiotics usage and becomes one major sticking point.[5]

Up to date, capillary electrophoresis and liquid chromatography coupled to different detectors as conventional methods have been often used for the detection of antibiotics, holding high sensitivity and selectivity.[6−8] However, their operation procedures are complicated, time-consuming, and costly, which hinder their on-site applications.[9,10] In the past years,

some alternative methods for quantification have been developed, such as electrochemistry,[11] fluorescence,[12] luminescence,[13] and surface-enhanced Raman scattering (SERS).[14−16] Among these alternative methods, SERS is considered a powerful analytic tool for chemical analysis, providing abundant molecular information and high sensitivity.[17] It is accepted that the strong enhancement signal can be attributed to the electromagnetic (EM) and chemical enhancement effects.[18] Specifically, hybrids of plasmonic metals with semiconductor oxides (such as ZnO) have received considerable attention. Compared with individual plasmonic SERS substrates, the introduction of semiconductor oxides improves the SERS sensitivity from the charge transfer (CT) effect, as well as the EM effect. Meanwhile, semiconductor oxides have a
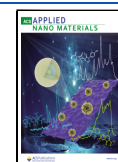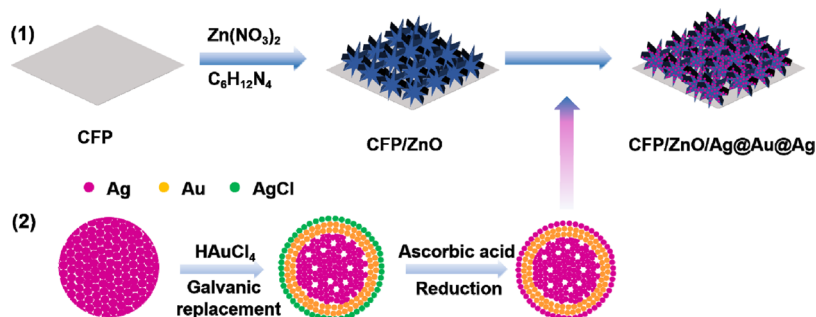
Scheme 1. Schematic of the Fabrication of CFP/ZnO/Ag@Au@Ag

stronger ability to adsorb analytes than plasmonic metals.[19−21] Moreover, since the nanogaps in SERS substrates can provide abundant "hotspots," multilayered nanostructures with controllable nanogaps can generate the coupling of mutual polariton modes.[22−24] Hao et al.[22] reported that 5-fold-twinned Ag−Au−Ag nanorods (NRs) had an enhancement factor (EF) of 9.0×10^5 for SERS detection of 2-naphthalenethiol. Zha et al.[23] synthesized a Ag-multilayer-Au film with a limit of detection (LOD) of 10^{-13} M for rhodamine 6G (R6G) detection. However, it is currently challenging to simply synthesize multilayered plasmonic nanostructures.

Usually, most of the above hybrids are supported on rigid supports, such as glass, silicon, and aluminum sheets. However, tedious sample preparation steps are often required for conventional rigid SERS substrates, which limits the applications for routine laboratory and on-site analysis.[25] Thus, flexible SERS substrates have gained popularity in recent years.[26,27] Especially, paper or paper-like chips as SERS sensing platforms have been extensively focused on.[28−35] Besides the merits of flexibility, portability, and cheapness, the porous nature provides the feasibility of rapid enrichment and concentration of analytes. Physical synthesis methods like soaking,[28] inkjet printing,[29] screening printing,[30] and filtration[31] are generally used for the fabrication of paper chips. Yet, only van der Waals binding to bound the nanomaterials onto paper always suffers from aggregation and poor adhesion.[33−35]

Based on the above backgrounds, in situ hydrothermal synthesis of three-dimensional (3D) ZnO nanoflowers (NFs) on cellulose filter paper (CFP) was followed by sequential deposition of Ag, Au, and Ag (Ag@Au@Ag, three-layered structures) via subsequent chemical reduction. Such a technique is particularly appealing for quick enrichment and ultrasensitive SERS detection due to a number of characteristics: (1) Since there are no surfactants used in the synthesis process, there will be no chance of noise or signal interference. (2) Due to cellulose's ability to maintain (14)-linked D-glucose units,[36] which bind ZnO with chemical bonds, the flexible SERS substrate demonstrates outstanding mechanical resilience even when folded and subjected to ultrasonication. (3) In light of the aforementioned contexts, three-dimensional (3D) ZnO nanoflow. The 3D nanostructure of ZnO NFs, the CT effect of ZnO−plasmonic metal, and EM coupling of three-layered plasmonic metals (Ag@Au@Ag) are responsible for the high SERS activity and stability, which is supported by finite difference time domain (FDTD) simulation analysis. When used in conjunction with the mobile phone−portable Raman spectrometer integrated system, ppb-level antibiotics in urine can be quickly identified without any prior treatment. (4) By simply soaking in the analyte solution, cellulose capsule-

action wicking allows for the 10 min fast SERS detection of three antibiotics (AMO, CIP, and TTC). The three antibiotics in urine can be successfully identified using principal component analysis (PCA) and linear discriminant analysis (LDA), which are intended for health monitoring and medication safety. Therefore, the high sensitivity, quick enrichment, and robust durability of the SERS paper chip are designed with practical applications for health monitoring and medication safety in mind.

■ MATERIALS AND METHODS

Materials. Zinc acetate dehydrate ($Zn(CH_3COO)_2 \cdot 2H_2O$), zinc nitrate hexahydrate ($Zn(NO_3)_2 \cdot 6H_2O$), and hexamethylenetetramine ($C_6H_{12}N_4$), silver nitrate ($AgNO_3$), sodium citrate, rhodamine 6G (R6G), and ascorbic acid (AA) were purchased from Sinopharm Chemical Reagent Co., Ltd. AMO, CIP, and TTC were obtained from the National Institute for Food and Drug Control. All reagents were of analytical grade and used without further purification. Water used in all experiments was purified by using a Millipore Q system.

Characterization. The nanostructures of the as-prepared materials were analyzed by field emission scanning electron microscopy (FE-SEM, JSM6701 F, JEOL Inc., Japan). High-resolution transmission electron microscopy (HR-TEM) was performed on a transmission electron microscope (TEM, Tecnai G2 F30, FEI). X-ray powder diffraction (XRD) analysis was performed on a Rigaku D/max-2400 (Cu Kα radiation, λ = 0.1541 nm) in a 2θ range from 10 to 90°. The UV−vis spectra were recorded on a UV−vis spectrophotometer (UV-2600, Shimadzu). The crystal surface composition was investigated by X-ray photoelectron spectroscopy (XPS, Kratos-AXIS ULTRA DLD).

Synthesis Process. The synthesis scheme of CFP/ZnO/Ag@Au@Ag is illustrated in the (1) process of Scheme 1.

First, the CFP/ZnO chip was synthesized in the following process: A 2×2 cm^2 piece of CFP was rinsed in ethanol and then dried with nitrogen gas. To form a uniform seed layer, a ZnO seed solution was prepared by dissolving 30 mM $Zn(CH_3COO)_2$ in 30 mL of ethanol at 60 °C. The CFP chip was coated with the seed solution drop by drop at 110 °C and subsequently placed into a thermal oven at 150 °C for 5 h. To vertically grow ZnO NFs, a growth solution was prepared by dissolving 25 mM $Zn(NO_3)_2$ and 25 mM $C_6H_{12}N_4$ in 100 mL of water at room temperature under stirring for 2 h. The seed-coated CFP was immersed into the growth solution and transferred to a 100 mL Teflon-lined stainless steel autoclave and maintained at 150 °C for 4 h. The ZnO NFs were in situ grown on the CFP, which was named CFP/ZnO. Finally, the CFP/ZnO chip was removed from the solution, washed with water, and dried in N₂.

Second, Ag nanoparticles (NPs) were loaded on CFP/ZnO via citrate reduction: 10 mL of $AgNO_3$ (0.2 M) solution was mixed with 10 mL of sodium citrate (0.05 M) solution at 60 °C under stirring. A few minutes later, one CFP/ZnO chip was put and reacted at 90 °C for 1 h. Finally, the chip was taken out, washed with water, and dried in N₂. CFP/ZnO with Ag loading was named CFP/ZnO/Ag.
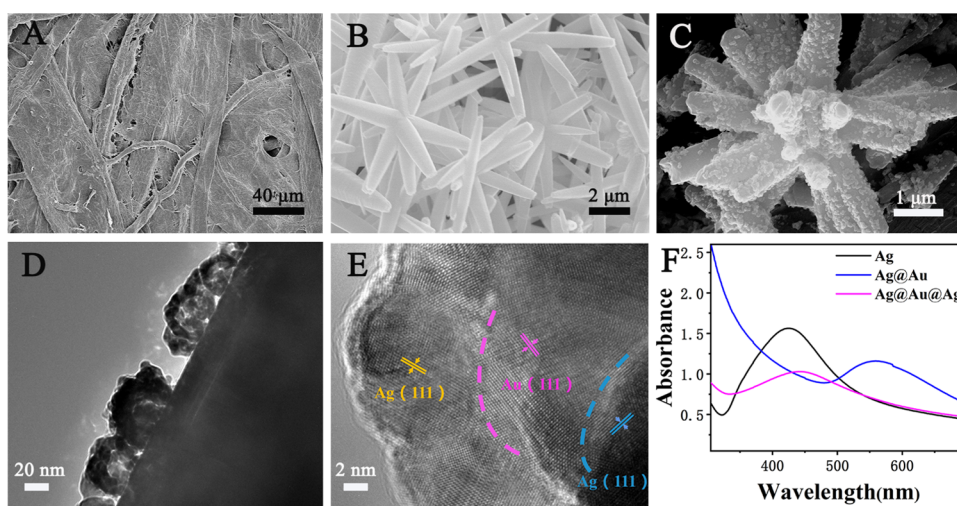
Figure 1. SEM images of pristine CFP (A), CFP/ZnO (B), and CFP/ZnO/Ag@Au@Ag (C). TEM (D) and HR-TEM (E) images of CFP/ZnO/Ag@Au@Ag. (F) UV−vis spectra of Ag, Ag@Au, and Ag@Au@Ag synthesized as illustrated in the (2) process of Scheme 1.

Third, three-layered plasmonic metal was synthesized as illustrated in the (2) process of Scheme 1. CFP/ZnO/Ag was immersed in 2.0 mL of $HAuCl_4$ (of 1 mM) for 10 min via the galvanic replacement reaction: $3Ag(s) + AuCl_4^-(aq) \rightarrow Au(s) + 3AgCl(s) + Cl^-(aq)$. The chip was taken out, washed with water, and dried in N_2, which was named CFP/ZnO/Ag@Au@AgCl. Then, 0.01 M ascorbic acid (AA) was used for further reduction of AgCl for 10 min via the reduction reaction: $AgCl(s) + e^- \rightarrow Ag(s) + Cl^-(aq)$. The chip loaded with three-layered plasmonic metals was named CFP/ZnO/Ag@Au@Ag. To obtain CFP/ZnO/Ag@Au, the CFP/ZnO/Ag@Au@AgCl substrate was washed with 1 M $NH_3 \cdot H_2O$ to remove AgCl.

In addition, ZnO/Ag@Au@Ag was deposited on the CFP by the simple soaking method, where ZnO/Ag@Au@Ag heterostructures were synthesized under the same procedure without the usage of CFP. To monitor the change of the SPR band, the Ag@Au@Ag heterostructures were synthesized according to the (2) process of Scheme 1 without the usage of CFP and ZnO.

Numerical Simulations. The EM field distributions were calculated using the finite difference time domain (FDTD) method. The electric field with linear polarization was incident on the nanosphere at the normal angle for calculation. The perfect matching layers were used to avoid the boundary reflections around structures under an incident power of 1 W and a work wavelength of 532 nm. The number of cells is controlled at about 10 000, and the average cell mass was 0.7622. The dielectric function of gold was taken from a multicoefficient fitting model of experimental data.[37] We considered the surrounding medium as the water solution with the refraction index $n = 1.33$ for all nanostructures.

SERS Detection. All Raman spectra were recorded on a Raman system (Zolix Finder Vista-HiR) except for special notes: 532 nm laser, 0.50 mW power, 1 μm diameter laser point, 100× L objective, and 10 s acquisition time. For each measurement, optical focusing was created. Three times repeated measurements were taken to record each Raman spectrum.

For R6G detection, the CFP/ZnO/Ag@Au@Ag chips were dipped in an aqueous R6G solution with different concentrations.

After folding for various lengths of time, paper chips adsorbed with 1.0 M R6G were found for the folding test. One folding time was accounted for when the paper chip was wrapped into a cylinder and then spread out. For the antidestruction test, the chips were subjected to ultrasonication under a power output of 200 W for different times. After that, the chips were adsorbed with 1.0 μM R6G for the SERS measurement.

For quantitative detection, the concentrations of AMO, CIP, and TTC from 10^{-4} to 10^{-9} M were adopted as the standard solutions. The real urine samples were collected from a normal adult, followed by dilution 100 times with water. A defined amount of AMO, CIP,

and TTC was added to the above urine samples to further calculate the recovery and relative standard deviation (RSD).

To examine the effect of interference, a series of inorganic and organic species (1 mM) were separately added to the aqueous antibiotic solution (0.1 mM). The paper chip was immersed into the solution spiked with interfering species for SERS measurements under the same conditions.

For portable detection, a 3D printed holder was installed in the Raman probe of the portable apparatus RMS1000 (Laser: 785 nm, Shanghai Oceanhood Optoelectronics Technology Co., Ltd, China) to fix the paper chip. Its aim is to find and fix the optimum focusing position. Three antibiotics (AMO, CIP, and TTC) in urine samples were tested on a common mobile phone with Test Program software.

■ RESULTS AND DISCUSSION

Characterization. The synthesis of CFP/ZnO/Ag@Au@Ag includes two sections: hydrothermal synthesis of ZnO NFs and deposition of a three-layered plasmonic metal on ZnO. A framework of cellulosic fibers can be seen on the surface of pristine CFP (Figure 1A). High-density ZnO NFs are distributed on the surface, where the NFs are assembled with many nanorods (Figure 1B). From the TEM image (Figure S1A), it can be observed that the nanorod has a diameter of ∼500 nm and a length of ∼3 μm. Clear lattice fringes of 0.28 nm can be seen in the HR-TEM image (Figure S1B), which corresponds to the ZnO(100) crystal plane of the orthorhombic structure.[38] The XRD pattern (Figure S1C) further reveals the formation of ZnO. The detailed analysis can be seen in the Supporting Information. Due to abundant hydroxyl groups of cellulose to anchored zinc ions through Zn-O bond chelation,[39] uniform growth of ZnO NFs is observed.

Three-layered plasmonic (Ag@Au@Ag) NPs were deposited on ZnO NFs via successive chemical reduction (the (2) process of Scheme 1). Figure 1C shows the SEM image of ZnO/Ag@Au@Ag, where numerous small NPs are uniformly decorated on the ZnO NFs. The TEM image (Figure 1D) shows that the NPs of roughly 40 nm in size are made up of a solid middle layer, an inner core that is porous, and an outside shell. The formation of the porous core is due to a typical galvanic replacement reaction.[40] The HR-TEM image (Figure 1E) further reveals a three-layered nanostructure. While the Au(111) phase in the middle layer has about 10 nm, the lattice spacing corresponding to the Ag (111) plane can be clearly
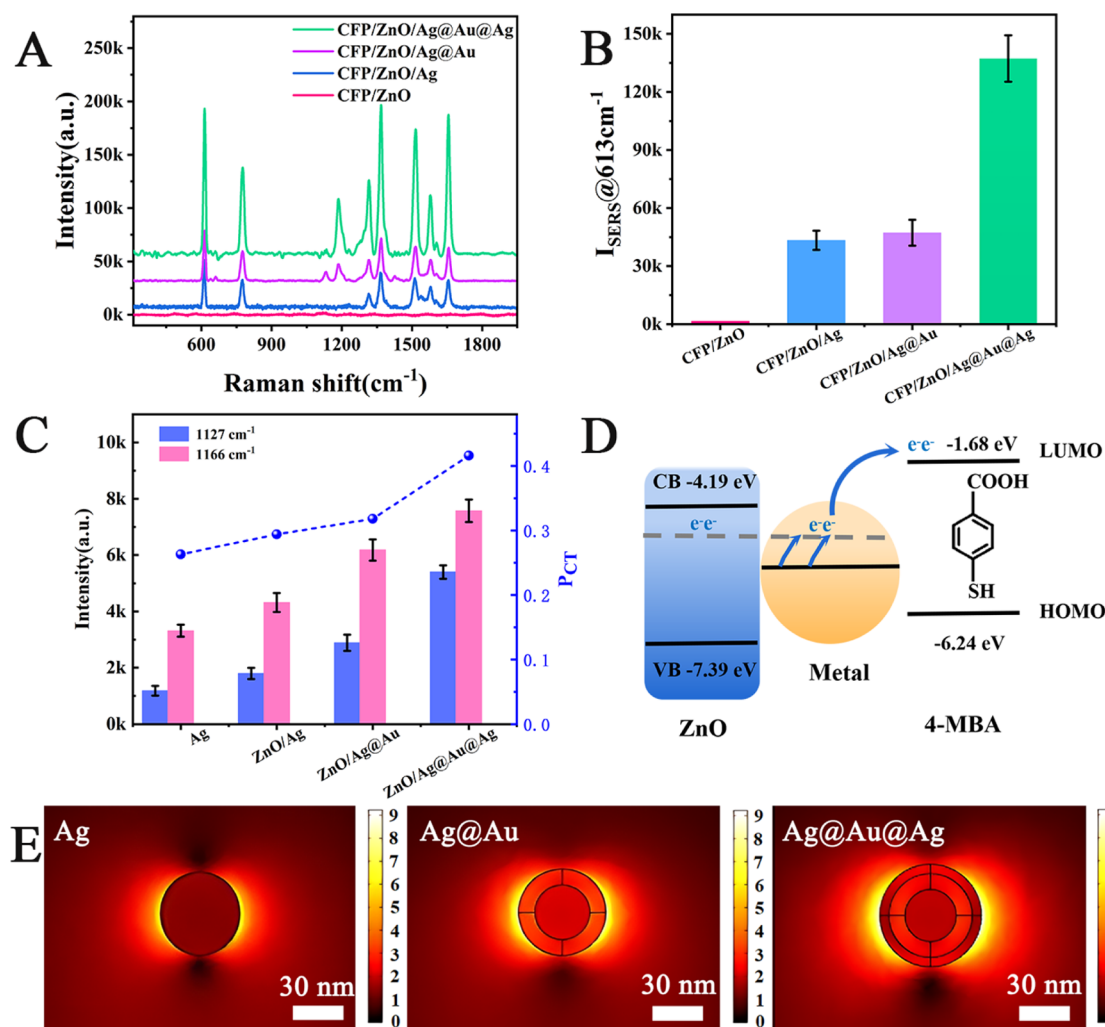
Figure 2. (A) SERS spectra of R6G (0.1 μM) adsorbed on CFP/ZnO, CFP/ZnO/Ag, CFP/ZnO/Ag@Au, and CFP/ZnO/Ag@Au@Ag and (B) the corresponding peak intensities at 613 cm^{-1}. (C) The peak intensity at 1127(I^k(CT)) and 1166(I^0(SPR)) cm^{-1} and the P_{CT} value (right) with different substrates. (D) Schematic diagram for the CT process between ZnO, Ag@Au@Ag, and the probe molecules (4-MBA as the example). (E) Electric field distribution based on FDTD simulations for Ag, Ag@Au, and Ag@Au@Ag.

seen in both the inner core of about 30 nm and the outer layer of about 3 nm. The EDX mapping (Figure S2) demonstrates the dispersion of these elements (Zn, Ag, and Au), where the Zn element spreads on the nanorod, while Ag and Au elements are sparsely dispersed together.

Due to the interference of CFP in the UV−vis measurement, we measured the UV−vis spectra of Ag, Ag@Au, and Ag@Au@Ag colloids, which were synthesized using the same procedures without the addition of CFP and ZnO. As depicted in Figure 1F, the localized surface plasmon resonance (LSPR) band is located at 424 nm for Ag colloids, representing the LSPR of Ag. After the galvanic replacement, the LSPR wavelength shifts to 556 nm, which belongs to the intrinsic LSPR of Au. This proves that the Au layer is coated on the Ag colloids. Via further reduction reaction with AA, the band appears at 438 nm again, which confirms the formation of the outer Ag layer. The UV−vis measurement proves the formation of three-layered plasmonic nanostructures (Ag@Au@Ag). We also investigated the UV−vis spectra of Zno@Ag, Zno@Ag@Au, and Zno@Ag@Au@Ag colloids that were synthesized using identical techniques but without the inclusion of CFP due to the interference of CFP in the UV−vis measurement (Figure S3).

XPS measurements were carried out to analyze the composition of CFP/ZnO/Ag@Au@Ag. In the survey spectrum (Figure S4A), Zn, O, Ag, and Au can be observed. High-resolution XPS spectra of the corresponding elements (Zn 2p, O 1s, Ag 3d, and Au 4f) can be seen in Figure S4B−E. The detailed analysis can be referred to in the Supporting Information. Its crystal structure was analyzed by XRD. In Figure S5, the ZnO diffraction peaks can be distinctly found, which presents the orthorhombic structure of ZnO (JCPDS Card No. 36-1451). Additionally, three diffraction peaks of Ag−Au are shown, corresponding to face-centered cubic (fcc) lattices. It is noted that each face has a single peak, since Au and Ag have similar lattice parameters of 4.0782 and 4.0862 Å, respectively.[41]

SERS Mechanism Study. The above characterization confirms special three-layered nanostructures decorated on ZnO NFs, so an enhanced SERS response is expected. R6G was selected as the probe molecule to evaluate the SERS activity. Figure 2A shows the SERS spectra of R6G adsorbed on CFP/ZnO, CFP/ZnO/Ag, CFP/ZnO/Ag@Au, and CFP/ZnO/Ag@Au@Ag. For pristine CFP/ZnO, there is nearly no Raman signal of R6G, indicating the SERS inertness of CFP/ZnO. After decorating Ag NPs on ZnO, characteristic peaks of
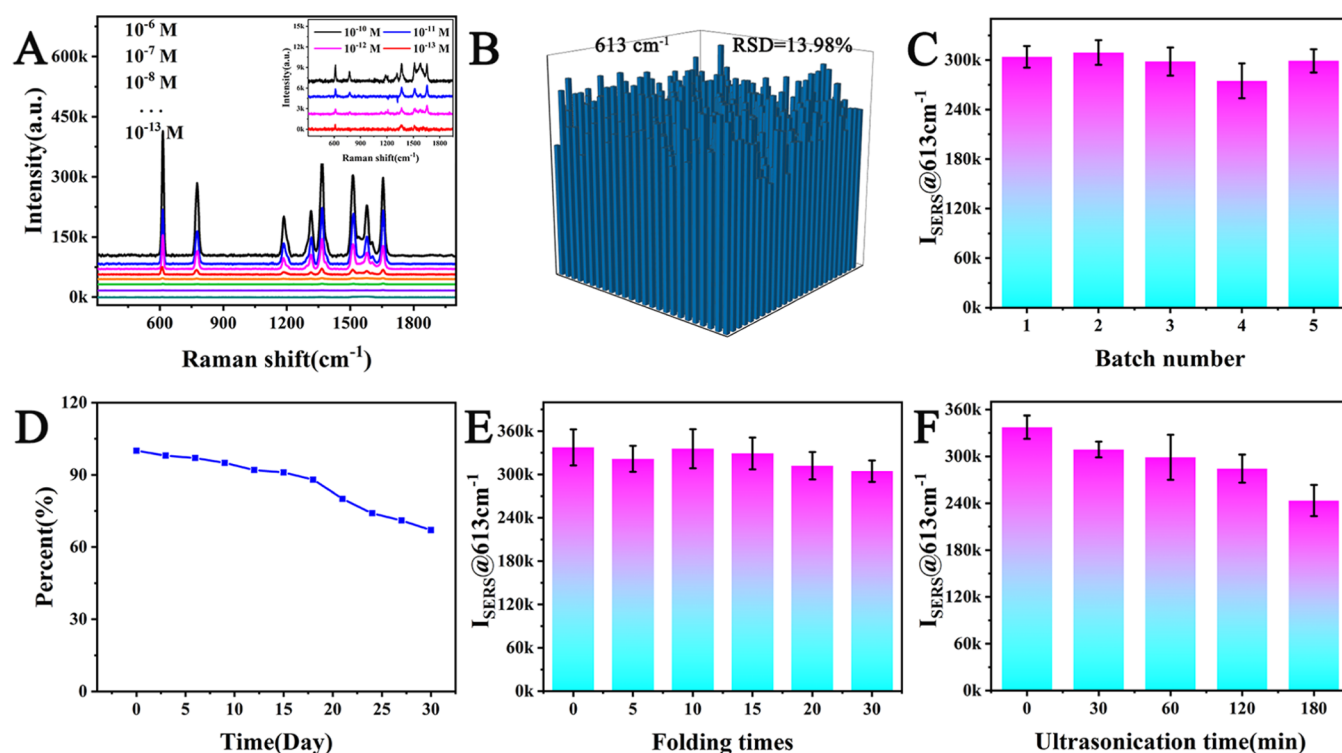
Figure 3. (A) SERS spectra of R6G with different concentrations. Raman mapping (B) and batch-to batch (C) uniformity. (D) SERS stability during a one month period. Effects of folding times (E) and ultrasonication time (F) on the peak intensity@ 613 cm^{-1}. Error bars indicate the standard deviation for the five measurements.

R6G can be clearly found on CFP/ZnO/Ag, which is similar to our previous work of ZnO/Ag nanorods as a prominent SERS substrate.[19] The enhanced Raman signal of R6G can be attributed to both the synergistic CT effect of ZnO−metal and the EM effect of Ag.

To understand the CT enhancement mechanism, the P_{CT} index is introduced, which is an important index to quantitatively evaluate the CT effect. 4-MBA was selected as the probe molecule due to its individual molecular bands reflecting the CT resonance. The SERS spectra of 4-MBA adsorbed on different substrates are shown in Figure S6. The P_{CT} calculation process is detailed in the Supporting Information. The specific calculation process is listed in Table S1. In view of the target peak intensity (Figure 2C), the Raman intensity of CFP/ZnO/Ag@Au@Ag is almost twice that of CFP/Ag@Au@Ag. Similarly, the Raman characteristic peak intensity of CFP/ZnO/Ag is also twice that of CFP/Ag. Importantly, the P_{CT} values of metals supported on ZnO are still higher than those of pristine metals (Figure 2C). These fully demonstrate that the ZnO support not only has the ability to disperse metal nanoparticles but also can bring a strong CT enhancement through the ZnO−metal−molecule system. The CT enhancement mechanism can be described in Figure 2D. The introduction of ZnO promotes electrons congregated at the surface of ZnO to inject into the Fermi level (E_f) of the metal, which leads to the balance charges at the junction of the metal and ZnO, thus forming an elevated E_f of the metal.[42] The photogenerated electrons can be more easily transferred from the new E_f of the metal to the lowest unoccupied molecular orbital (LUMO) level of the 4-MBA molecule. Accordingly, a stronger SERS response is obtained after the introduction of ZnO.

In addition, the three-layered nanostructure has the ability to cause the EM coupling effect, which results in a considerably enhanced electric field and a stronger SERS signal.[24] Using 613 cm^{-1} as the calibration (Figure 2B), the peak intensity of CFP/ZnO/Ag@Au@Ag is about 3.0 times that of CFP/ZnO/Ag; CFP/ZnO/Ag@Au has a stronger Raman intensity than CFP/ZnO/Ag. For a better understanding of the special nanostructure on the SERS performance, we calculated the EM field when the Gaussian beam is incident normally using the FDTD method. The EM field distributions on the $x−y$ plane for the three structures at 532 nm excitation are shown in Figure 2E. Compared to other structures, the EM field surrounding Ag@Au@Ag is stronger. This can be attributed to the shift in the LSPR band caused by the EM coupling in the three-layered nanostructure. Ag@Au@Ag's falling edge of the absorption spectrum is where the excitation wavelength of 532 nm is located; therefore, excited SERS signals are not reabsorbed by strong LSPR resonance.

Basic SERS Performance and Mechanical Durability. Based on the above optimized conditions, basic SERS performances of CFP/ZnO/Ag@Au@Ag including sensitivity, stability, and reproducibility were tested by reusing R6G as the probe molecule. Figure 3A shows the SERS spectra of R6G in the concentration range from 10^{-6} to 10^{-13} M. It is noted that the characteristic Raman signal at 10^{-13} M can be identified. The LOD is calculated to be 10^{-13} M for R6G detection from the inset of Figure 3A. Additionally, the EF was calculated to be 5.68 × 10^8 using the 613 cm^{-1} peak as the calibration. The detailed calculation process is described in the Supporting Information and Figure S8.

The SERS uniformity was also accessed by using Raman mapping. The Raman mapping measurement is described in detail, as shown in the Supporting Information. The intensity
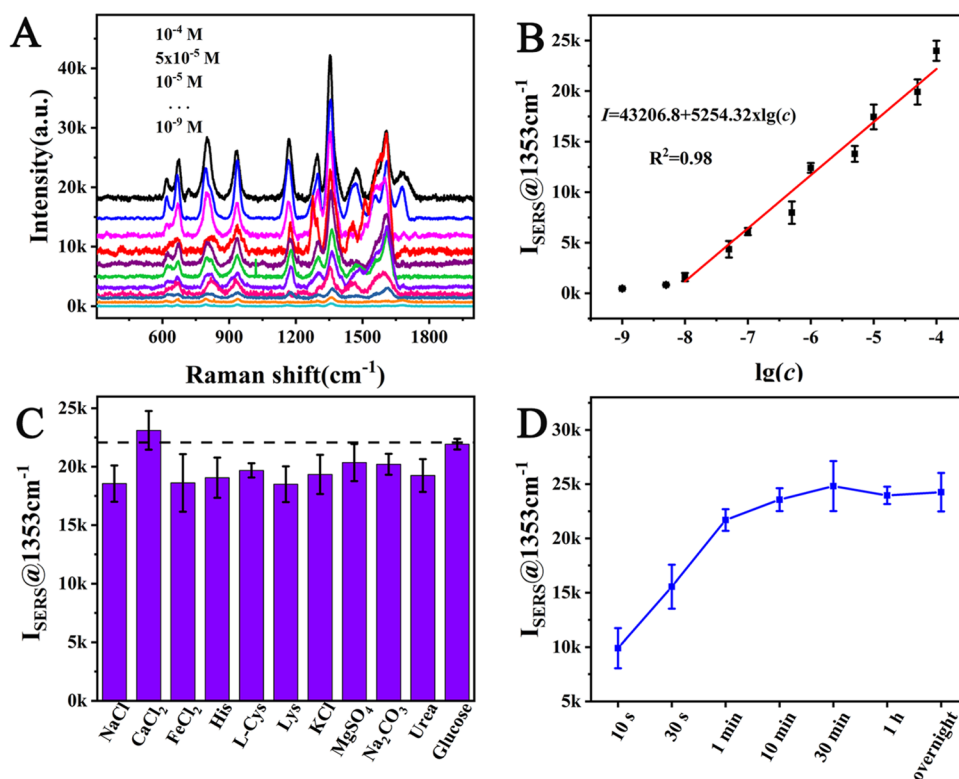
Figure 4. (A) SERS spectra of AMO with different concentrations on CFP/ZnO/Ag@Au@Ag. (B) The relationship is linear plots between the peak intensities of AMO and the logarithm of their concentrations. (C) The SERS intensities of AMO (0.1 mM) in the presence of the interfering reagents were 1 mM for each. The corresponding peak intensities at 613 cm^{-1} of AMO (D).

distribution of R6G @613 cm^{-1} in a 12 × 12 μm^2 area is shown in Figure S7. The corresponding histogram of peak intensities is displayed in Figure 3B, where the RSD is 13.98%. The uniform growth of ZnO/Ag@Au@Ag on CFP and the resulting formation of a large number of uniform and effective hotspots is responsible for the good SERS uniformity.[43]

To examine the reproducibility, five different production batches were determined. The corresponding SERS spectra are shown in Figure S9A. The RSD is 5.1% from the peak intensities at 613 cm^{-1} (Figure 3C). The stability test is necessary for Ag-based SERS substrates. The chip adsorbed with 1 μM R6G was stored in air and measured every 3 days under the same conditions. The corresponding SERS spectra are displayed in Figure S9B. The peak intensities at 613 cm^{-1} decrease to a certain degree. Nonetheless, the peak intensity still has 67% of the initial intensity after 30 days (Figure 3D). On the contrary, pure Ag colloids had only 40% of the initial intensity after 30 days in air.[22] The above tests on sensitivity, uniformity, reproducibility, and stability demonstrate that the SERS paper chip exhibits great potential in practical applications.

Mechanical durability is another significant factor in practical applications. Hand folding and ultrasonication are powerfully damaging forces, particularly for paper chips. The paper chip's SERS activity for the treatment of hand folding remains constant even after 30 folds (Figures 3E and S10A in the Supporting Information). As for powerful ultrasonication, the CFP/ZnO/Ag@Au@Ag chip still maintains 71% SERS intensity of the initial after 180 min of ultrasonication (Figure 3F). The original SERS spectra are presented in Figure S10B. By contrast, when the CFP was physically modified with ZnO/Ag@Au@Ag via soaking, the SERS signal almost disappeared

after 60 min of ultrasonication (Figure S11). The study shows that ZnO can attach to CFP by means of a chemical connection with Zn−O.[44] So, the in situ synthesis strategy is the most significant factor to obtain strong mechanical durability for SERS applications.

SERS Detection of Antibiotics. Quantitative SERS detection of AMO was performed on the paper chips, where the adsorption time was 10 min. Figure 4A shows the SERS spectra of AMO with a series of concentrations. The intensities of the characteristic Raman peaks are expected to decrease with a decrease in its concentration. Selecting the peaks at 1353 cm^{-1} (AMO) as the calibration (Figure 4B), a linear curve between the peak intensity and the logarithm of the concentration is obtained, where the linear range is from 0.01 to 100 μM. Meanwhile, the LOD reaches up to 1 nM for AMO detection. Compared with previous detection methods such as electrochemistry,[45] colorimetry,[46,47] and SERS,[48−51] our SERS detection method holds wider linear ranges and lower LODs in the detection of AMO (Table 1). Furthermore, the selectivity was determined by adding various inorganic salts (NaCl, Na$_2$CO$_3$, MgSO$_4$, KCl, FeCl$_2$, CaCl$_2$) and organic compounds (Lys (lysine), His (histidine), L-Cys (L-cystine), urea, and glucose) with 1 mM into aqueous AMO solutions (0.1 mM). As compared to the control solution, there are only 15% fluctuations of the individual characteristic peak intensity for the addition of the interfering species (Figure 4C).

The AMO detection in real samples was performed by the standard addition method. The known concentrations were spiked into human urine samples, and then the calculated concentrations were obtained using the above linear equations. The detection results are listed in Table S4. The recoveries for

Table 1. Comparison of the LODs for AMO Detection between this SERS Assay and Those from Previous Studies

material	method	LOD	ref
CuBi$_2$O$_4$	electrochemistry	0.2 mM	[45]
Qt Ag NPs	colorimetry	4.46 μM	[46]
Cu−GO nanocomposites	colorimetry	1.71 mM	[47]
Ag colloids	SERS	50 mM	[48]
silver-coated polymeric microbeads	SERS	10 nM	[49]
microfluidic SERS	SERS	2.7 nM	[50]
Ag NCs	SERS	0.41 mM	[51]
CFP/ZnO/Ag@Au@Ag	SERS	1 nM	this work

AMO detection are limited from 90 to 106%, and all of the RSDs are limited to around 10%.

Furthermore, the capillary-action wicking of CFP and the strong adsorption ability of ZnO give a chance for rapid enrichment of the analytes, possibly achieving rapid SERS detection. The CFP-based substrate was first cut into small paper strips with 0.5 × 0.5 cm^2. Then, the paper strips were separately immersed into the AMO solutions for different times. The effect of the adsorption time of the analyte was studied. The SERS spectra are displayed in Figure S12. Using the individual characteristic peak (1353 cm^{-1}), one can see from Figure 4D that the peak intensities increase with the adsorption time. It is found that the peak intensity of 10 min adsorption is almost equal to the intensity overnight (>96%). The adsorption equilibrium can be achieved within 10 min for AMO. Li et al. reported SERS detection of antibiotics within

10 min under the electrophoretic preconcentration.[52] The extraction of TTC in milk was done in 20 min by using a potentiostat to apply a fixed potential to accelerate the enrichment process. By contrast, our operation was simple, where the paper chip was soaked into the analyte solution for 10 min and dried in air for SERS detection.[53]

Similarly, the other two antibiotics (CIP and TTC) could be detected sensitively, selectively, and rapidly based on CFP/ZnO/Ag@Au@Ag. The detailed analysis processes can be seen in Figures S13 and S14 in the Supporting Information. For CIP and TTC, the linear equations are given in Table S2. Both linear ranges are from 0.05 to 100 μM, along with both LODs of 10 nM. Good selectivity is also achieved against inorganic salts and organic compounds for the detection of the two antibiotics. Importantly, rapid SERS detection was also done within 10 min adsorption for CIP and TTC.

Portable Detection and Identification by PCA-LDA Analysis. Portable SERS analysis is one of the most efficient routes to achieving on-site detection. It is significant for the operators to easily and conveniently complete the operation, especially outdoors. In this study, a portable Raman spectrometer (laser wavelength of 785 nm) was linked to a common mobile phone for portable detection (Figure 5A). The paper chip was fixed using a 3D printed holder on the device probe to find and fix the optimum focusing position (inset of Figure 5A). Once fixing the position, the operators only inserted a new paper chip into the holder for the next measurement.

Figure S15A−C shows the SERS spectra of the antibiotics (AMO, CIP, and TTC) at different concentrations from 10
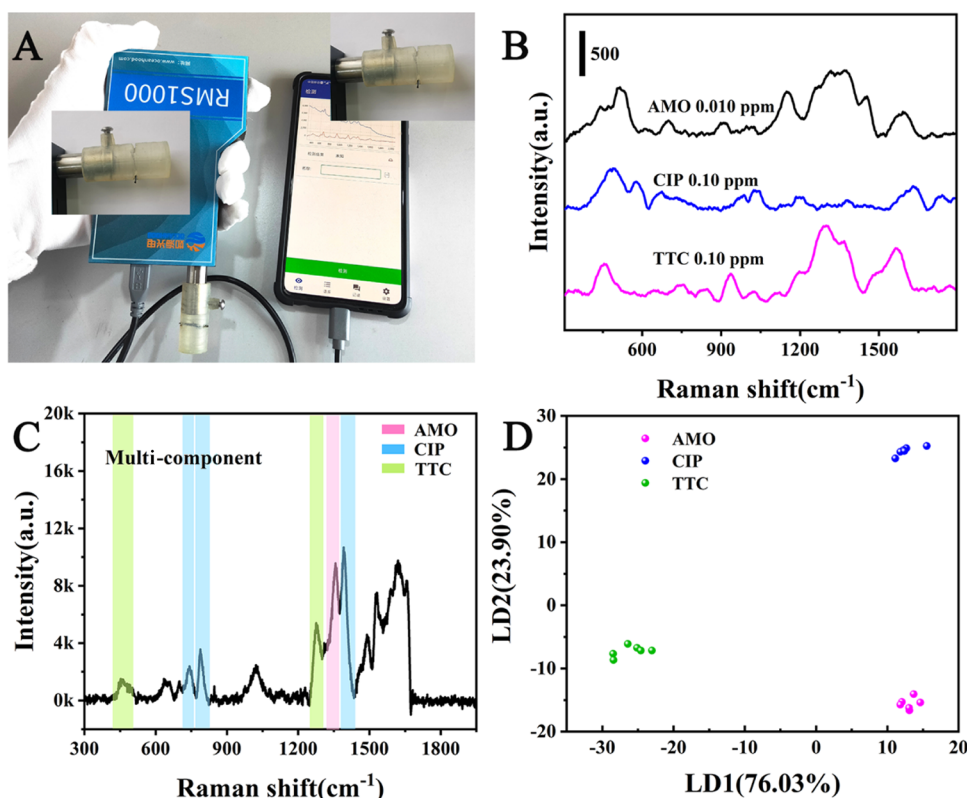

Figure 5. (A) Photograph of the portable detection apparatus with a 3D printed holder to fix the paper chip. (B) SERS spectra of parts per billion level AMO, CIP, and TTC obtained by the portable detection apparatus. (C) SERS spectra of multiple components of three antibiotics (AMO, CIP, and TTC). (D) LDA plot of LD1 versus LD2 computed from the SERS spectra of the three antibiotics. Integration time: 10 s; laser power: 10 mW; laser wavelength: 785 nm.

ppm to 10 ppb, which were measured on the portable Raman spectrometer. As shown in Figure 5B, the detectable concentrations of AMO, CIP, and TTC are 0.01, 0.1, and 0.1 ppm, respectively. The detection ability can serve the needs of the maximum residue limit (MRL, 100 ppb) of antibiotics in food products by the Food and Drug Administration (FDA) of the European Union and other countries.[54,55] It is expected that the paper chip decorated with 3D ZnO NFs and three-layered plasmonic nanostructures possesses great potential for point-of-care (POC) detection in the field analysis of various hazardous materials in the near future.

SERS is considered a powerful analytical tool to provide a unique vibrational fingerprint and exhibit molecularly narrow band spectra. So, it has been popular and promising to detect multiple components in a matrix for the past few years.[16,56] Herein, three kinds of antibiotics (AMO, CIP, and TTC) were mixed in a solution. The integrated SERS spectrum is shown in Figure 5C. The characteristic bands of AMO (1353 cm^{-1}), CIP (748, 789, and 1391 cm^{-1}), and TTC (460 and 1282 cm^{-1}) could be markedly distinguished. Nevertheless, it is laborious to artificially identify the three antibiotics from their SERS spectra. Rapid identification of three antibiotics is necessary by combining this with PCA-LDA analysis. PCA is one of the most widely used multivariate statistical techniques in reducing the dimensionality of correlated multivariate data.[28,55] We performed PCA analysis of the SERS spectra (initial dimension = 1625) to reduce the dimensionality (Figure S16). The first 29 principal components are used as input to LDA for classification, and the results are shown in Figure 5D. The SERS spectra of AMO, CIP, and TTC can be categorized into three individual and noninterfering clusters. The discrimination accuracy is close to 100%. Distinctly, the components of the three antibiotics could be rapidly and efficiently identified from the SERS spectra with the aid of PCA-LDA analysis.

CONCLUSIONS

A SERS paper chip was developed for rapid, sensitive, and portable detection of the three antibiotics (AMO, CIP, and TTC) in urine samples. 3D ZnO NFs were in situ grown on the CFP, and then three-layered plasmonic nanostructures (Ag@Au@Ag) were deposited on the ZnO NFs via successive chemical reduction with any surfactants. The in situ synthesis strategy improved the mechanical durability. FDTD analysis confirmed that the three-layer plasmonic nanostructures significantly enhanced the electrical field intensity. High sensitivity was realized with LODs of 1, 10, and 10 nM for the SERS detection of AMO, CIP, and TTC, respectively. Owing to the capillary-action wicking of CFP and the strong adsorption ability of ZnO, 10 min SERS detection of the antibiotics was achieved. Aiming at the on-site detection of paper chips, ppb-level antibiotics were successfully detected without any pretreatment using the portable Raman spectrophotometer−mobile phone integrated system. The three antibiotics with similar SERS signals could be efficiently identified with PCA-LDA analysis. The bifunctional paper chip with rapid enrichment and high sensitivity is expected to have great potential for the POC detection and discrimination of multiple components with similar molecular structures.

ASSOCIATED CONTENT

Supporting Information

The Supporting Information is available free of charge at https://pubs.acs.org/doi/10.1021/acsanm.3c03467.

TEM and XRD of ZnO NRs; EDX spectrum; high-resolution XPS spectra; SERS spectra of the stability and uniformity; Raman mapping; EF calculation; mechanical durability; mechanical stability on physical fabrication; and LOD comparison (PDF)

AUTHOR INFORMATION

Corresponding Authors

Yuee Li − *School of Information Science and Engineering, Lanzhou University, Lanzhou 730000, China;* ⊙ orcid.org/0000-0001-5430-1587; Email: liyuee@lzu.edu.cn

Weichun Ye − *State Key Laboratory of Applied Organic Chemistry and Department of Chemistry, Lanzhou University, Lanzhou 730000, China;* ⊙ orcid.org/0000-0003-1690-5720; Email: yewch@lzu.edu.cn

Yumin Li − *Key Laboratory of Digestive System Tumors, Lanzhou University, Lanzhou 730000, China;* Email: liym@lzu.edu.cn

Hua Zhang − *State Key Laboratory of Environmental Geochemistry, Institute of Geochemistry, Chinese Academy of Sciences, Guiyang 550081, China;* Email: zhanghua@mail.gyig.ac.cn

Authors

Juanjuan Yan − *State Key Laboratory of Applied Organic Chemistry and Department of Chemistry, Lanzhou University, Lanzhou 730000, China*

Morui Wang − *School of Information Science and Engineering, Lanzhou University, Lanzhou 730000, China*

Huaiqin Yin − *State Key Laboratory of Applied Organic Chemistry and Department of Chemistry, Lanzhou University, Lanzhou 730000, China*

Mengmeng Ma − *State Key Laboratory of Applied Organic Chemistry and Department of Chemistry, Lanzhou University, Lanzhou 730000, China*

Haiyuan Hu − *State Key Laboratory of Solid Lubrication, Lanzhou Institute of Chemical Physics, Chinese Academy of Sciences, Lanzhou 730000, China*

Complete contact information is available at:
https://pubs.acs.org/10.1021/acsanm.3c03467

Author Contributions

[#]J.Y., M.W., and H.Y. contributed equally to this work.

Notes

The authors declare no competing financial interest.

ACKNOWLEDGMENTS

■ REFERENCES

(1) Giske, C. G. Contemporary resistance trends and mechanisms for the old antibiotics colistin temocillin, fosfomycin, mecillinam and nitrofurantoin. *Clin. Microbiol. Infect.* **2015**, *21*, 899−905.

(2) Sukul, P.; Spiteller, M. Fluoroquinolone antibiotics in the environment. *Rev. Environ. Contam. Toxicol.* **2007**, *191*, 131−162.

(3) Deusenbery, C.; Wang, Y.; Shukla, A. Recent innovations in bacterial infection detection and treatment. *ACS Infect. Dis.* **2021**, *7*, 695−720.

(4) Kovalakova, P.; Cizmas, L.; McDonald, T. J.; Marsalek, B.; Feng, M.; Sharma, V. K. Occurrence and toxicity of antibiotics in the aquatic environment: a review. *Chemosphere* **2020**, *251*, No. 126351.

(5) Lan, L.; Yao, Y.; Ping, J.; Ying, Y. Recent advances in nanomaterial-based biosensors for antibiotics detection. *Biosens. Bioelectron.* **2017**, *91*, 504−514.

(6) Delvaux, C.; Dauvin, M.; Boulanger, M.; Quinton, L.; Mengin-Lecreulx, D.; Joris, B.; De Pauw, E.; Far, J. Use of capillary zone electrophoresis coupled to electrospray mass spectrometry for the detection and absolute quantitation of peptidoglycan-derived peptides in bacterial cytoplasmic extracts. *Anal. Chem.* **2021**, *93*, 2342−2350.

(7) Faulkner, D. V.; Cantley, M. L.; Kennedy, D. G.; Elliott, C. T.; Crooks, S. R. H. MRM3-based UHPLC-MS/MS method for quantitation of total florfenicol residue content in milk and withdrawal study profile of milk from treated cows. *Food Chem.* **2022**, *379*, No. 132070.

(8) Pérez-Lemus, N.; Lopez-Serna, R.; Perez-Elvira, S. I.; Barrado, E. Analysis of 60 pharmaceuticals and personal care products in sewage sludge by ultrahigh performance liquid chromatography and tandem mass spectroscopy. *Microchem. J.* **2022**, *175*, No. 107148.

(9) Yan, S.-R.; Foroughi, M. M.; Safaei, M.; Jahani, S.; Ebrahimpour, N.; Borhani, F.; Baravati, N. R.; Aramesh-Boroujeni, Z.; Foong, L. K. A review: Recent advances in ultrasensitive and highly specific recognition aptasensors with various detection strategies. *Int. J. Biol. Macromol.* **2020**, *155*, 184−207.

(10) Li, S.; Liu, X.; Chai, H.; Huang, Y. Recent advances in the construction and analytical applications of metal-organic frameworks-based nanozymes. *TrAC, Trends Anal. Chem.* **2018**, *105*, 391−403, DOI: 10.1016/j.trac.2018.06.001.

(11) Pakapongpan, S.; Poo-Arporn, Y.; Tuantranont, A.; Poo-Arporn, R. P. A facile one-pot synthesis of magnetic iron oxide nanoparticles embed N-doped graphene modified magnetic screen printed electrode for electrochemical sensing of chloramphenicol and diethylstilbestrol. *Talanta* **2022**, *241*, No. 123184.

(12) Zhang, J.; Shi, G. Rational design of MoS_2 QDs and Eu^{3+} as a ratiometric fluorescent probe for point-of-care visual quantitative detection of tetracycline via smartphone-based portable platform. *Anal. Chim. Acta* **2022**, *1198*, No. 339572.

(13) Yang, G.; Jiang, X.; Xu, H.; Zhao, B. Applications of MOFs as luminescent sensors for environmental pollutants. *Small* **2021**, *17*, No. 2005327.

(14) Guo, Y.; Girmatsion, M.; Li, H.; Xie, Y.; Yao, W.; Qian, H.; Abraha, B.; Mahmud, A. Rapid and ultrasensitive detection of food contaminants using surface-enhanced Raman spectroscopy-based methods. *Crit. Rev. Food Sci. Nutr.* **2021**, *61*, 3555−3568.

(15) Jiao, A.; Cui, Q.; Li, S.; Li, H.; Xu, L.; Tian, Y.; Ma, H.; Zhang, M.; Liu, X.; Chen, M. Aligned TiO_2 nanorod arrays decorated with closely interconnected Au/Ag nanoparticles: Near-infrared SERS active sensor for monitoring of antibiotic molecules in water. *Sens. Actuators, B* **2022**, *350*, No. 130848, DOI: 10.1016/j.snb.2021.130848.

(16) Lee, K. H.; Jang, H.; Kim, Y. S.; Lee, C. H.; Cho, S. H.; Kim, M.; Son, H.; Bae, K. B.; Dao, D. V.; Jung, Y. S.; Lee, I. H. Synergistic SERS enhancement in GaN-Ag hybrid system toward label-free and multiplexed detection of antibiotics in aqueous solutions. *Adv. Sci.* **2021**, *8*, No. 2100640.

(17) Hu, W.; Xia, L.; Hu, Y.; Li, G. Recent progress on three-dimensional substrates for surface-enhanced Raman spectroscopic analysis. *Microchem. J.* **2022**, *172*, No. 106908.

(18) Schlücker, S. Surface-enhanced Raman spectroscopy: Concepts and chemical applications. *Angew. Chem., Int. Ed.* **2014**, *53*, 4756−4795.

(19) Liu, C.; Xu, X.; Wang, C.; Qiu, G.; Ye, W.; Li, Y.; Wang, D. ZnO/Ag nanorods as a prominent SERS substrate contributed by synergistic charge transfer effect for simultaneous detection of oral antidiabetic drugs pioglitazone and phenformin. *Sens. Actuators, B* **2020**, *307*, No. 127634, DOI: 10.1016/j.snb.2019.127634.

(20) Wang, C.; Xu, X.; Qiu, G.; Ye, W.; Li, Y.; Harris, R. A.; Jiang, C. Group-targeting SERS screening of total benzodiazepines based on large-size (111) faceted silver nanosheets decorated with zinc oxide nanoparticles. *Anal. Chem.* **2021**, *93*, 3403−3410.

(21) Tiwari, M.; Singh, A.; Dureja, S.; Basu, S.; Pattanayek, S. K. Au nanoparticles decorated $ZnO/ZnFe_2O_4$ composite SERS-active substrate for melamine detection. *Talanta* **2022**, *236*, No. 122819.

(22) Hao, H.; Yang, Y.; Zou, C.; Chen, W.; Wen, H.; Wang, W.; Yang, Y. Effects of strain and kinetics on the H_2O_2-assisted reconstruction of Ag-Au-Ag nanorods. *Langmuir* **2020**, *36*, 9770−9779.

(23) Zha, Z.; Liu, R.; Yang, W.; Li, C.; Gao, J.; Shaf, M.; Fan, X.; Li, Z.; Du, X.; Jiang, S. Surface-enhanced Raman scattering by the composite structure of Ag NP-multilayer Au films separated by Al_2O_3. *Opt. Express* **2021**, *29*, 8890−8901.

(24) Jin, L.; She, G.; Li, J.; Xia, J.; Wang, X.; Mu, L.; Shi, W. A facile fabrication of Ag-Au-Ag nanostructures with nanogaps for intensified surface-enhanced Raman scattering. *Appl. Surf. Sci.* **2016**, *389*, 67−72.

(25) Li, Y.; Zhang, K.; Zhao, J.; Ji, J.; Ji, C.; Liu, B. A three-dimensional silver nanoparticles decorated plasmonic paper strip for SERS detection of low-abundance molecules. *Talanta* **2016**, *147*, 493−500.

(26) Luo, J.; Wang, Z.; Li, Y.; Wang, C.; Sun, J.; Ye, W.; Wang, X.; Shao, B. Durable and flexible Ag-nanowire-embedded PDMS films for the recyclable swabbing detection of malachite green residue in fruits and fingerprints. *Sens. Actuators, B* **2021**, *347*, No. 130602, DOI: 10.1016/j.snb.2021.130602.

(27) Ouyang, L.; Yao, L.; Zhou, T.; Zhu, L. Accurate SERS detection of malachite green in aquatic products on basis of graphene wrapped flexible sensor. *Anal. Chim. Acta* **2018**, *1027*, 83−91.

(28) Huang, D.; Zhuang, Z.; Wang, Z.; Li, S.; Zhong, H.; Liu, Z.; Guo, Z.; Zhang, W. Black phosphorus-Au filter paper-based three-dimensional SERS substrate for rapid detection of foodborne bacteria. *Appl. Surf. Sci.* **2019**, *497*, No. 143825.

(29) Tay, L. L.; Poirier, S.; Ghaemi, A.; Hulse, J. Inkjet-printed paper-based surface enhanced Raman scattering (SERS) sensors for the detection of narcotics. *MRS Adv.* **2022**, *7*, 190−196.

(30) Li, D.; Cao, X.; Zhang, Q.; Ren, X.; Jiang, L.; Li, D.; Deng, W.; Liu, H. Facile *in situ* synthesis of core-shell MOF@Ag nanoparticle composites on screen-printed electrodes for ultrasensitive SERS detection of polycyclic aromatic hydrocarbons. *J. Mater. Chem. A* **2019**, *7*, 14108−14117.

(31) Xu, F.; Shang, W.; Xuan, M.; Ma, G.; Ben, Z. Layered filter paper-silver nanoparticle-ZIF-8 composite for efficient multi-mode enrichment and sensitive SERS detection of thiram. *Chemosphere* **2022**, *288*, No. 132635.

(32) Kim, W.; Lee, S. H.; Kim, J. H.; Ahn, Y. J.; Kim, Y. H.; Yu, J. S.; Choi, S. Paper-based surface-enhanced Raman spectroscopy for diagnosing prenatal diseases in women. *ACS Nano* **2018**, *12*, 7100−7108.

(33) Xie, L.; Zeng, H.; Zhu, J.; Zhang, Z.; Sun, H.; Xia, W.; Du, Y. State of the art in flexible SERS sensors toward label-free and onsitedetection: from design to applications. *Nano Res.* **2022**, *15*, 4374−4394.

(34) Huo, D.; Chen, B.; Meng, G.; Huang, Z.; Li, M.; Lei, Y. Ag-nanoparticles@bacterial nanocellulose as a 3D flexible and robust surface-enhanced Raman scattering substrate. *ACS Appl. Mater. Interfaces* **2020**, *12*, 50713−50720.

(35) Tanis, S. N.; Ilhan, H.; Guven, B.; Tayyarcan, E.; Ciftci, K. H.; Saglam, N.; Boyaci, I. H.; Tamer, U. A disposable gold-cellulose

nanofibril platform for SERS mapping. *Anal. Methods* **2020**, *12*, 3164−3172.

(36) Kang, H.; Liu, R.; Huang, Y. Cellulose-based gels. *Macromol. Chem. Phys.* **2016**, *217*, 1322−1334.

(37) Wei, Y.; Kong, J.; Yang, L.; Ke, L.; Tan, H. R.; Liu, H.; Du, H.; et al. Polydopamine-assisted decoration of ZnO nanorods with Ag nanoparticles: an improved photoelectrochemical anode. *J. Mater. Chem. A* **2013**, *1*, 5045−5052.

(38) Ye, Z.; Li, C.; Celentano, M.; Lindley, M.; O'Reilly, T.; Greer, A. J.; Huang, Y.; Hardacre, C.; Haigh, S. J.; Xu, Y.; Bell, S. E. J. Surfactant-free synthesis of spiky hollow Ag-Au nanostars with chemically exposed surfaces for enhanced catalysis and single-particle SERS. *JACS Au* **2022**, *2*, 178−187.

(39) Kumar, S.; Baruah, A.; Tonda, S.; Kumar, B.; Shanker, V.; Sreedhar, B. Cost-effective and eco-friendly synthesis of novel and stable N-doped ZnO/g-C_3N_4 core-shell nanoplates with excellent visible-light responsive photocatalysis. *Nanoscale* **2014**, *6*, 4830−4842.

(40) Liu, R.; Guo, J.; Ma, G.; Jiang, P.; Zhang, D.; Li, D.; Chen, L.; Guo, Y.; Ge, G. Alloyed crystalline Au−Ag hollow nanostructures with high chemical stability and catalytic performance. *ACS Appl. Mater. Interfaces* **2016**, *8*, 16833−16844.

(41) Johnson, P. B.; Christy, R. W. Optical Constants of the Noble Metals. *Phys. Rev. B* **1972**, *6*, 4370−4379.

(42) Wang, Y.; Liu, J.; Zhao, X.; Yang, C.; Ozaki, Y.; Xu, Z.; Zhao, B.; Yu, Z. A chiral signal-amplified sensor for enantioselective discrimination of amino acids based on charge transfer-induced SERS. *Chem. Commun.* **2019**, *55*, 9697−9700.

(43) Xu, F.; Shang, W.; Ma, G.; Zhu, Y.; Wu, M. Metal organic framework wrapped gold nanourchin assembled on filter membrane for fast and sensitive SERS analysis. *Sens. Actuators, B* **2021**, *326*, No. 128968, DOI: 10.1016/j.snb.2020.128968.

(44) Zheng, M.; Wang, P. L.; Zhao, S. W.; Guo, Y. R.; Li, L.; Yuan, F. L.; Pan, Q. J. Cellulose nanofiber induced self-assembly of zinc oxide nanoparticles: Theoretical and experimental study on interfacial interaction. *Carbohydr. Polym.* **2018**, *195*, 525−533.

(45) Dumitru, R.; Negrea, S.; Păcurariu, C.; Surdu, A.; Ianculescu, A.; Pop, A.; Manea, F. $CuBi_2O_4$ Synthesis, Characterization, and application in sensitive amperometric/voltammetric detection of amoxicillin in aqueous solutions. *Nanomaterials* **2021**, *11* (3), No. 740, DOI: 10.3390/nano11030740.

(46) ul Ain, N.; Anis, I.; Ahmed, F.; Shah, M. R.; Parveen, S.; Faizi, S.; Ahmed, S. Colorimetric detection of amoxicillin based on querecetagetin coated silver nanoparticles. *Sens. Actuators, B* **2018**, *265*, 617−624, DOI: 10.1016/j.snb.2018.03.079.

(47) Anh, N. T.; Dinh, N. X.; Tuan, H. V.; Doan, M. Q.; Anh, N. H.; Khi, N. T.; Trang, V. T.; Tri, D. Q.; Le, A. T. Eco-friendly copper nanomaterials-based dual-mode optical nanosensors for ultrasensitive trace determination of amoxicillin antibiotics residue in tap water samples. *Mater. Res. Bull.* **2022**, *147*, No. 111649.

(48) Clarke, S. J.; Littleford, R. E.; Smith, W. E.; Goodacre, R. Rapid monitoring of antibiotics using Raman and surface enhanced Raman Spectroscopy. *Analyst* **2005**, *130* (7), 1019−1026, DOI: 10.1039/b502540k.

(49) Kibar, G.; Topal, A. E.; Dana, A.; Tuncel, A. Newly designed silver coated-magnetic, monodisperse polymeric microbeads as SERS substrate for low-level detection of amoxicillin. *J. Mol. Struct.* **2016**, *1119*, 133−138.

(50) Wang, L.; Zhou, G.; Guan, X. L.; Zhao, L. Rapid preparation of surface-enhanced Raman substrate in microfluidic channel for trace detection of amoxicillin. *Spectrochim. Acta, Part A* **2020**, *235*, No. 118262, DOI: 10.1016/j.saa.2020.118262.

(51) Dikmen, G. Ultrasensitive detection of amoxicillin using the plasmonic silver nanocube as SERS active substrate. *Spectrochim. Acta, Part A* **2022**, *278*, No. 121308, DOI: 10.1016/j.saa.2022.121308.

(52) Li, Y.-T.; Qu, L.; Li, D.; Song, Q.; Fathi, F.; Long, Y. Rapid and sensitive *in-situ* detection of polar antibiotics in water using a disposable Ag-graphene sensor based on electrophoretic preconcentration and surface-enhanced Raman spectroscopy. *Biosens. Bioelectron.* **2013**, *43*, 94−100.

(53) Sereshti, H.; Karami, F.; Nouri, N.; Farahani, A. Electrochemically controlled solid phase microextraction based on a conductive polyaniline-graphene oxide nanocomposite for extraction of tetracyclines in milk and water. *J. Sci. Food Agric.* **2021**, *101*, 2304−2311.

(54) Granados-Chinchilla, F.; Rodriguez, C. Tetracyclines in food and feeding stuffs: from regulation to analytical methods, bacterial resistance, and environmental and health implications. *J. Anal. Methods Chem.* **2017**, *2017*, No. 1315479.

(55) Pogurschi, E.; Ciric, A.; Zugrav, C.; Patrascu, D. Identification of antibiotic residues in raw milk samples coming from the metropolitan area of bucharest. *Agric. Agric. Sci. Procedia* **2015**, *6*, 242−245, DOI: 10.1016/j.aaspro.2015.08.066.

(56) Li, J.; Yan, H.; Tan, X.; Lu, Z.; Ha, H. Cauliflower-inspired 3D SERS substrate for multiple mycotoxins detection. *Anal. Chem.* **2019**, *91*, 3885−3892.